

LINEAR ANALYSIS OF THE DYNAMICS OF NEURAL MASSES

WALTER J. FREEMAN

Walter J. Freeman Journal Article e-*Reprint*
 Reprinted from ANNUAL REVIEW OF BIOPHYSICS AND BIOENGINEERING, Vol. 1, 1972
 This work was supported by NIMH Grant MH 06686.
 cc: CREATIVE COMMONS COPYRIGHT: [Attribution-Share alike Licence](https://creativecommons.org/licenses/by-sa/4.0/)
 Original PDF File Source: <http://sulcus.berkeley.edu/FreemanWWW/manuscripts/IA3/72.html>

This review is concerned with the problem of how to identify and characterize masses of neurons empirically as dynamic entities that have properties related to but distinct from those of the component neurons. This can only be done by observing and measuring experimentally the responses of neural masses to known stimuli. But measurement presupposes some theoretical framework to provide the necessary basis functions and the units. For example, a value for frequency is predicated on the presence of a periodic wave-form; a rate constant presumes an exponential decay; a numerical estimate of dispersion requires some distribution function; and so forth. The purpose of this review is to suggest that linear systems analysis can provide a very useful structure for measuring compound neural responses and for comprehending some of the elementary underlying dynamics. It does not define the entities nor explain what they do or how they do it. It merely provides the basis for measurement, which is the first step beyond uncorrelated observations and the prerequisite for testing theories of neural masses.

WHAT IS A NEURAL MASS?

Granted that nervous systems are composed of neurons, the most compelling fact about even the simpler brains is that the numbers of neurons are extremely large. Because the neuron is conceived as the elementary unit of neural function, and because it is accessible to measurement by an array of microtechniques, the proper aim of neurophysiology is the analysis of brain function in terms of the properties of single neurons. Yet most of what is known about the operation of the brain in relation to behavior has come from studies based on stimulation (electrical or chemical), field potential recordings, or ablation (by selective surgery or disease) of masses of brain tissue containing tens or hundreds of millions of neurons. The conceptual gap between the functions of single neurons and those numbers of neurons is still very wide.

TABLE 1. Numbers of neurons in logarithmic scale*

Number	Structure	Domain of Observation
10,000,000,000	Neurons, human brain	
1,000,000,000	Neurons, cat brain	Behavior:
	Visual cortex, Area 17, man	Stimulation
	Primary olfactory axons, cat	and ablation
100,000,000	Olfactory bulb, cat	
10,000,000	Olfactory cortex, cat	
	Evoked potential, bulbar at threshold	
	Neurons/mm ³ , cerebellum	
1,000,000	Optic nerve, man	Neural masses:
	Neurons, crustacean	Field potentials
	Neurons/mm ² , bulb, cat	
100,000	Mitral cells, cat	
	Spinal ganglion, man	
10,000	PON fibers at threshold for AEP	
1,000	Visceral ganglion, Aplysia	Networks:
	Retina, <i>Lizinus</i>	Unit recording
	Optic nerve, <i>Necturus</i>	and analysis
100	Sympathetic ganglion, rat	
10	Cardiac ganglion, <i>Homarus</i>	

TABLE 1 - Some examples are listed on a logarithmic scale of estimated numbers of neurons in some common preparations. From references 1-5 and the author's unpublished data.

The parts of nervous systems accessible to experimental observation may be arranged in a logarithmic scale, as in Table 1, which contains examples of estimated numbers of neurons in some well-known preparations (1-3). Listed in the lower third of the table, extending roughly from 10^1 to 10^4 neurons, are some isolatable parts of invertebrate nervous systems, including the cardiac ganglion of the lobster (2), the eye of the horseshoe crab (5), and the visceral ganglion of the sea-snail (4). To those might be added the monosynaptic sensorimotor relays of the vertebrate spinal cord (6). These are systems for which the relatively small numbers of neurons have offered hope of analysis and understanding by models based on discrete networks of single simulated neurons.

The upper third of the scale, 10^1 to 10^{11} neurons, is represented by structures from the vertebrate brain, which on surgical removal or destruction by disease leave recognizable and reproducible deficits in behavior, such as anosmia, cortical blindness, hemiplegia, etc (7).

Between these levels is a range of numbers, 10^4 to 10^7 neurons, which are too few to leave notable behavioral deficits on ablation, unless they comprise a projection pathway such as the optic nerve. On the other hand the numbers are too great to conceive of modeling in terms of networks of finite numbers of cells. This is the region over which a conceptual span is needed, to account for the behaviorally related properties of brains in terms of single neurons. It is the domain of neural masses.

WHY USE LINEAR SYSTEMS ANALYSIS?

The neural masses in the central numerical region can be conceived empirically as occupying a few mm^2 of cortical surface, or a few mm^3 of nuclear volume in the brain stem or spinal cord. They have three properties of particular interest in the present context.

First, the output of a neural mass is often accessible to measurement as a holistic event, such as a compound action potential of a nerve trunk, a field of potential in the volume of the mass owing to the extracellular spread and summation of dendritic current, or some derivative event such as the strength of a muscle contraction. For neural masses in the brain the electrical field potentials may be the single most valuable source of information about their dynamic properties, because they manifest the weighted instantaneous sum of extracellular potentials generated by large numbers of neurons. The problems of determining the locations, distributions, and active states of neurons in the masses generating such fields have been discussed in numerous articles and reviews (8-13), and the subject is still grossly underdeveloped. Yet it seems undeniable that such events, when properly analyzed, provide an essential key to the understanding of neural masses.

Second, the output of neural masses characteristically is graded over the physiological range of function. Output is proportional to input, within limits, and the responses to two or more inputs are additive. This set of properties was explored and documented in quantitative detail by Sherrington (14-16) in his studies of reflex mechanisms in the brain stem and spinal cord, which were the immediate precursor for the analysis of the synaptic potentials of neurons by use of the intracellular microelectrode (6, 17, 18). Sherrington described his principle results as demonstrating the algebraic summation of excitatory and inhibitory influences in the neurons of the spinal cord.

These properties imply that within appropriate limits of amplitude, the operations of neural masses conform to the principle of superposition, and to that extent their dynamics can be described by means of linear differential equations. The principle has been directly verified for spinal motoneurons by Granit (17) and is the basis for the quantitative analysis of the dynamics of the array of receptor neurons comprising the eye of *Limulus* (19, 20).

The relevance of these properties to some aspects of transmission in the higher nervous systems has been documented among others by Stark & Sherman (21) in the analysis of the pupillary reflex as a servomechanism; by Lopes da Silva (22), Cleland & Enroth-Cugell (23), Maffei (24), and Regan (25) in the analysis of visual cortical potentials evoked by sine wave modulated light; and by Tielen et al (26) in the observation of electrical responses of auditory cortex to sinusoidally modulated sound.

Third, neural masses are readily accessible to electrical stimulation with extracellular electrodes on peripheral afferent nerves or in the tracts, nuclei, and cortical surfaces of the brain. Characteristically such stimulation activates large numbers of axons in the vicinity of an electrode, i.e., it is a multicellular input leading to the activation of masses of neurons. Mathematically it can be approximated by a delta function in the time dimension although not in the spatial dimensions of the stimulus. This form of activation has the additional advantage of bypassing the receptors through which sinusoidal stimuli are delivered (21-26) and for which transfer functions are difficult to obtain.

These three properties form the basis for the expectation that some of the fundamental characteristics of neural masses might be described in terms of linear systems analysis. Very simply, the neural mass under study is subjected to an electrical pulse, which is superimposed on the background activity normally present in the input pathways to all neural masses. The output field potential, after suitable averaging to remove the background activity generated by the mass (comprising the EEG waves of the mass), is treated as the impulse response of the system.

By use of paired shocks or repetitive trains of stimuli (27, 28) a linear range of function is defined. In this range the impulse response can be treated as the sum of a set of terms, which are the solution to a set of linear differential equations having the boundary conditions corresponding to an impulse input (29). These terms serve to generate exponential curves and damped sine waves, which become the basis functions (30) or elementary curves required for measurement. An appropriate set is chosen by trial and error, and the sum is fitted by use of nonlinear regression to the digitized averaged evoked potential (AEP) or impulse response (31). The Laplace transform of the evaluated curve yields the linear differential equation best describing the dynamics of the neural mass in the designated experimental state.

The combination of electrical stimulation at some reproducible site with field potential recording near the center of some evoked activity provides a useful empirical description of a neural mass. Again, it does not provide a definition; it provides a platform for observation and measurement. The most effective use of the approach requires detailed specification of the anatomy of the stimulated tract and the target mass; of the spatial distribution of the field potential and its relation to the gross and microscopic structures of the generating neurons; identification of the neuron types responsible for unit and field potentials; and so forth. One of the seeming disadvantages of the use of evoked potentials and linear analysis is the heavy requirement for detailed correlative field mapping and histological measurement. On the contrary, even with initially poor specification of stimulus and recording conditions, which is usually the case in the beginning, it is easy to get immediate results, and to feed these back into the experiment as a basis for improving the specification. By successive modifications the initially hazy conception of the neural mass under study can and should become progressively more sharply defined and richly detailed.

HOW MIGHT LINEAR ANALYSIS BE APPLIED?

The derivation of transfer functions in this approach (thus far described) is of very limited value, owing to the fact that the waveforms of AEPs vary with changes in stimulus intensity. The amplitudes of responses change in linear proportion to the input intensity, but the coefficients describing the frequencies and exponential decay rates of the responses are often exquisitely sensitive to changes in the input magnitude.

The limitation with respect to amplitude is further reflected in the fact that the modulation amplitude for sinusoidal stimulation must in most cases be restricted to some fraction of a sustained "dc" input bias, e.g. on the order of 20% for visual cortex in dogs in response to sine wave modulated light (22). The limits are similar though less stringent for retinal ganglion cells and peripheral receptors, e.g. up to 60% for Limulus (20). When the limits are exceeded, harmonics become prominent, and the frequency-response curves tend to change with amplitude (32).

The principal reason for this pervasive nonlinearity in the function of neural masses lies in the limitations on output of the neurons in the masses over a range of input amplitudes. Sherrington described these limits (15) with the terms "facilitation" and "occlusion." The former was attributed to the threshold of each neuron and implied that two stimuli together might cause a neuron to discharge, whereas either alone might not. The latter was attributed to the refractory properties of neurons, such that if one stimulus caused a neuron to discharge, the addition of another stimulus too soon after the first would not augment its output.

More recently the nonlinearity has been described as bilateral saturation (22, 32-38). This is a static nonlinearity (35), which can be described as an amplitude-dependent property of neural masses. Conceptually the transference of the neural mass can be separated into a linear frequency-dependent part $C(s)$ and a nonlinear amplitude-dependent part $P(V)$. The latter function serves to specify the values for the coefficients of the former over a range of input magnitudes. In this manner, using linear differential equations having state-dependent coefficients, the linear systems approach can be extended to cover a broad range of dynamic function of neural masses, in so far as AEPs and their functional correlates are concerned (28, 39).

Additionally, owing to the fact that neurons in masses communicate within themselves by dendritic currents (often but not always giving rise to EEG waves and to AEPs) but between each other by propagated action potentials (spikes or pulses), it is essential to observe and measure the pulse trains of representative neurons. These are either random pulse trains of background activity or induced responses to electrical stimulation, which are best observed in the form of poststimulus time (PST) histograms. In either case, because observation is restricted to one or at most a few neurons at a time, it is necessary to assume that the performance of the neuron is representative of others in the mass, provided the period of observation is long enough. This quasi-ergodic hypothesis seems to work well enough for purposes of linear analysis, though how far it can be pushed is unclear. Simultaneously recorded EEG waves and background pulse trains on the one hand and of AEPs and PST histograms on the other constitute the essential raw materials for the analysis of the dynamics of neural masses.

IN WHAT WAY DOES THE MASS DIFFER FROM THE NEURON?

The neural mass is composed of neurons, and its properties have a generic resemblance to those of single neurons. But it is not identical to them, and its properties cannot be predicted or evaluated wholly from measurements on single neurons. This is partly because the properties of the mass depend to some extent on distributions of various parameters of single

neurons and partly because the properties of the mass depend on the massive connectivity of large numbers of neurons. Both of these facets are largely inaccessible to single-unit analysis.

In order to illustrate this proposition examples will now be given of the calculation of the amplitude-dependent transference $P(V)$, where V is wave amplitude, and the frequency-dependent transference $C(s)$, where s is the Laplacian operator, for the neural masses in the olfactory bulb and cortex of the cat and rabbit. These structures have been thoroughly studied both anatomically (40, 41) and electrophysiologically (28, 36-39, 42-48) and have been shown to be well suited to description using linear differential equations (34, 36, 48).

WHAT IS THE MEANING OF FORWARD GAIN?

Communication within and between neural masses is assumed here to be solely on the basis of synaptic transmission. This implies that in general a neural mass receives impulses of some space-time density and transmits impulses of some differing space-time density. Forward gain is defined as the ratio of the instantaneous magnitudes of output and input. Because both take the form of pulse density functions (pulses/unit time/unit area or volume) the gain is a dimensionless factor. However, each neural mass converts its pulse density input to a dendritic current or wave function and reconverts some spatio-temporally transformed wave function into another pulse density function. The conversion for each of the two stages must be described, the first in terms of the magnitude of pulse-to-wave conversion (P-V) and the second in terms of the magnitude of wave-to-pulse conversion (V-P). The product of the two magnitudes is the forward gain of the mass. In general there is a central amplitude range of function for both stages of a neural mass, in which the amplitude of output is proportional to that of input, and is additive as well, so that the conversions are linear. If the pulse density functions are estimated from the pulse frequencies of single-neuron pulse trains in pulses/second (pps), and the wave function is estimated from the amplitude of the extracellular field potential in microvolts (μV), then (P-V) and (V-P) conversions can be described using coefficients in units of $4V/pps$ and $pps/\mu V$ respectively. The product of the coefficients is the dimensionless gain.

In fact neither stage is linear over the achievable physiological range. Each conversion undergoes progressively stronger saturation with increasing departure from the central part of the range. The effect of saturation is to reduce the gain, so that forward gain is an amplitude-dependent nonlinearity (36, 38). The dependency of gain for the impulse response is on the input pulse magnitude or on the initial response amplitude, and the initial value for the gain holds throughout the duration of the impulse response. For this reason the nonlinearity is static and is readily susceptible to piece-wise linear approximation. It is then feasible to separate the frequency-dependent from the amplitude-dependent properties, and to describe the former with linear differential equations in time and the latter with linear differential equations in amplitude. Owing to the remarkable degree to which superposition holds in neural masses, these considerations are also valid for "spontaneous" or background activity. They do not hold for the full description of seizures or convulsive neural discharges, although the conditions for instability leading to seizures can be described (36, 48).

For (P-V) conversion the limits are imposed by the ionic mechanisms of dendritic current (49). The greater the membrane depolarization in response to an excitatory input, the less the difference between membrane potential and the equilibrium potential for the excitatory postsynaptic potential (EPSP). This reduces the effective electromotive force for the dendritic current operating into a high resistance current path, so the current increment is reduced proportionately for equal increases in excitatory input. At some level of input, were it achievable, the current would asymptotically approach a limiting value.²

²[The occasional failure of superposition of intracellular postsynaptic potentials and the demonstration that conductance changes in dendritic membrane are the basis for synaptic potentials (49) has led to the conclusion that variable membrane conductance can operate as an amplitude-dependent voltage divider for some neuronal geometries. This nonlinearity would give rise not only to saturation but also to variable passive membrane rate constants. Reasons have been given elsewhere (36) for believing that over the "physiological" range of function these rate constants are invariant. Therefore, it is concluded that even if the voltage divider effects can be demonstrated to hold for single neurons in some conditions, they do not account for the saturation effects observed in neural masses.]

The same properties hold for inhibition, except that the limit is closer to the resting state, because the difference between resting membrane potential and the equilibrium potential for the inhibitory postsynaptic potential (IPSP) is (from the illustrations cited in reference 49) roughly one-sixth that for the EPSP. The input-output curve for (P-V) conversion is therefore sigmoidal with sharper curvature on the inhibitory side (Figure 1, upper right: this graph must be viewed after rotation 90° counterclockwise, for the reason given below).

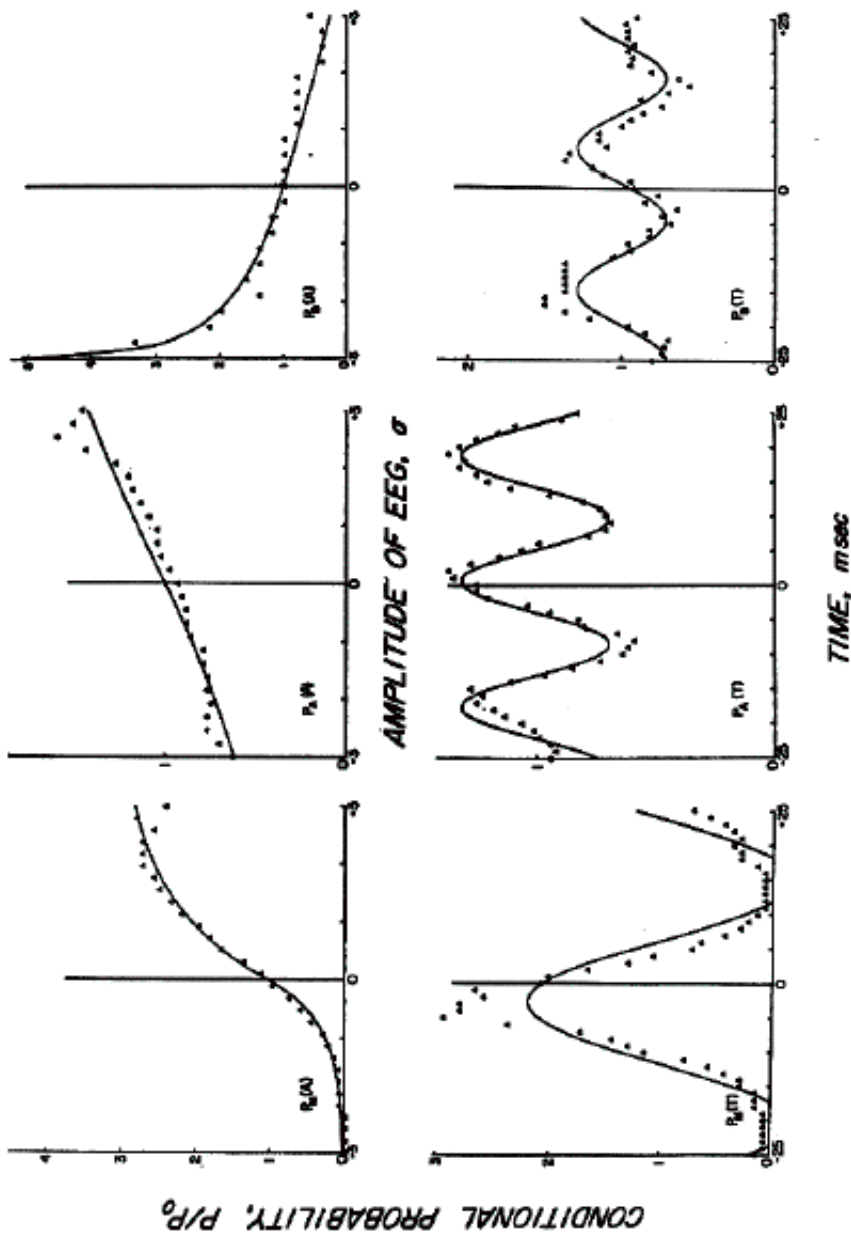


FIGURE 1 (instructions for reading these graphs should be followed upon orienting the time and amplitude abscissas in the horizontal plane). Above. The calculated curves in the three upper frames are the predicted input-output curves $P(A)$ of the olfactory neural masses. The derivatives of these curves suffice to describe the amplitude-dependent forward gains. The triangles are the pulse probability of single neurons conditional on the amplitude of EEG, $\hat{P}(A)$. P_0 is the mean pulse rate. The curves are: upper left—(V-P) conversion for type M cells (Equations 17 and 18); upper middle—(V-P) conversion for type A cells (Equations 17 and 18); upper right—(P-V) conversion for type B cells (rotate graph 90° counterclockwise, Equations 15 and 16). Below. Experimental [triangles, $\hat{P}(T)$] and theoretical [curves, $P(T)$] pulse probabilities conditional on time lag from EEG are shown. The EEG crest occurs at $T=0$. $P_M(T)$ leads the EEG; $P_A(T)$ shows a slight lag from the EEG, though on the average it is in phase; $P_B(T)$ lags the EEG.

The stage for (V-P) conversion is similarly bounded, on the inhibitory side by the thresholds for the trigger zones and on the excitatory side by the maximum mean sustained firing rate for the mass, which in turn is determined by the relative refractory periods and the hyperpolarizing and depolarizing after-potentials of the single neurons. For single neurons the relation between pulse output rate and imposed transmembrane current is linear or nearly so (17, 19, 32, 50) over a much wider range of pulse rates than is expected for a neural mass. There are two reasons for this. On the inhibitory side the thresholds or firing times for the mass are distributed (51-53). On the excitatory side neurons can be driven to very high pulse rates for brief periods, provided they are not challenged to fire during a subsequent rest period (37). For a neural mass the maximum firing rate must be computed over both active and rest periods. On these grounds the input-output curve for (V-P) conversion must also be sigmoidal, with sharper curvature on the inhibitory side (Figure 1, upper left).

HOW CAN PULSE-TO-WAVE CONVERSION BY DENDRITES BE QUANTIFIED?

The relationships between pulse input P and wave output V can be expressed in the form of two first-order differential equations, which state that the magnitude of output decreases in proportion to the rate of change in output with respect to input between two limiting values, V_i and V_e ,

$$\frac{dV}{dP} = -\zeta(V - V_i) \quad V < 0 \quad 1.$$

$$\frac{dV}{dP} = \frac{\zeta}{r_d}(V - V_e) \quad V > 0 \quad 2.$$

where $V_i (<0)$ is the level of extracellular wave potential corresponding to the inhibitory equilibrium potential for the dendritic membranes of the neurons generating the wave, and $V_e (>0)$ is the level of extracellular wave potential corresponding to the excitatory equilibrium potential. Both are expressed as the difference from extracellular rest potential, which is taken as zero for background activity. The empirical rate constants, ζ on the inhibitory side ($V < 0$) and ζ/r_d on the excitatory side, are in units of 1/pps, and r_d is dimensionless. The derivatives are set equal to each other at $V = 0$, so that

$$V_e = -r_d V_i \quad 3.$$

The solutions to the differential equations are

$$V = V_i(1 - \exp[-\zeta(P - \bar{P}_0)]) \quad P > \bar{P}_0, V < 0 \quad 4.$$

$$V = r_d V_i(1 - \exp[-\zeta/r_d(P - \bar{P}_0)]) \quad P < \bar{P}_0, V > 0 \quad 5.$$

where \bar{P}_0 (P with over-bar) is the overall mean pulse rate of the neural mass at $V = 0$.

HOW CAN WAVE-TO-PULSE CONVERSION BY AXONS BE QUANTIFIED?

For (V-P) conversion the rate of change in pulse output P with respect to wave input V is likewise characterized as proportional to the output:

$$\frac{dP}{dV} = r_a \gamma P \quad V < 0 \quad 6.$$

$$\frac{dP}{dV} = -\gamma P \quad V > 0 \quad 7.$$

where γ and $r_a \gamma$ are respectively excitatory and inhibitory rate constants in units of $1/\mu V$.

The solutions to the differential equations are

$$P = \bar{P}_0 e^{r_a \gamma V} \quad V < 0 \quad 8.$$

$$P = P_{\max} - (P_{\max} - \bar{P}_0) e^{-\gamma V} \quad V > 0 \quad 9.$$

$$P = \bar{P}_0 \quad V = 0 \quad 10.$$

The value for P_{\max} is found by setting the derivatives equal to each other at $V = 0$, and solving for P_{\max} :

$$\frac{dP}{dV} = r_a \gamma \bar{P}_0 e^{r_a \gamma V} \quad V < 0 \quad 11.$$

$$\frac{dP}{dV} = \gamma (P_{\max} - \bar{P}_0) e^{-\gamma V} \quad V > 0 \quad 12.$$

$$P_{\max} = \bar{P}_0 (r_a + 1) \quad V = 0 \quad 13.$$

Equation 9 then becomes

$$P = \bar{P}_0 + r_a \bar{P}_0 (1 - e^{-\gamma V}) \quad V > 0 \quad 14.$$

WHAT IS PULSE PROBABILITY CONDITIONAL ON WAVE AMPLITUDE?

The experimental evaluation of these two sets of equations 4-5 and 8-14 (54) is based on fitting curves generated from them to the pulse probability of single neurons in the olfactory bulb or cortex $^A P(T, A)$, conditional (55) on the amplitude and time of the EEG recorded from a closely neighboring point in the bulb or cortex.

The conditional probability tables are constructed from long records of EEG amplitudes and single-neuron pulse trains measured simultaneously at 1.0 msec intervals. Three correlations have been made. The first is between the pulse probability of the mitral and tufted cells in the olfactory bulb, $^A P_m(T, A)$, and the wave generated by the bulbar granule cells, $V_G(T)$ (40). The second is between the pulse probability of superficial pyramidal cells in the olfactory cortex, $^A P_A(T, A)$, and the wave generated by the same cells, $VA(T)$ (28, 39). The third is between the pulse probability of

cortical granule cells $\hat{P}_B(T, A)$ and $V_A(T)$ (37).

Owing to delays between the actions of the mitral-tufted and granule cells, and between types B and A neurons, it is essential to establish the optimum time lag T for each correlation. This is done by asking, for each measured pulse value (0 or 1), what is the value for wave amplitude in each of the 25 msec preceding the present value, and for each wave amplitude, what is the pulse value in each of the 25 msec preceding? For each time lag and amplitude value the total number of times a pulse occurred is divided by the total number of times the wave amplitude occurred. The resulting conditional probability $\hat{P}(T, A)$ is multiplied by 1000 to express it in pps. For graphic display it is divided by P_0 (mean pulse rate).

The EEG amplitude probability histogram for bulb and cortex almost always conforms to a normal density function with standard deviation a . The limits of the table, $\hat{P}(T, A)$, are placed at $\pm 3\sigma$ and at ± 25 msec. The pulse probability conditional on time, $\hat{P}(T)$, is determined by averaging across values for $\hat{P}(T, A)$ between $+1$ to 3σ for each value of T . The oscillatory time courses for $\hat{P}(T)$ have the same frequency as the dominant peak of the power spectrum of the EEG. The crests of $\hat{P}_m(T)$ lead the crest of the EEG by about one quarter cycle (at the center line in Figure 1, lower set); those for $\hat{P}_A(T)$ are in phase, and those for $\hat{P}_B(T)$ lag by about one quarter cycle.

The experimental pulse probability conditional on amplitude, $\hat{P}(A)$, is taken at time of the crest of $\hat{P}_m(T)$ preceding the EEG crest, at the crest of $\hat{P}_A(T)$ at the EEG crest, and at the trough of $\hat{P}_B(T)$ preceding the EEG crest (Figure 1, upper set).

The choice of equations for the curves $P(A)$ to fit these data is based on the premise that in all cases the independent variable is V , owing to the fact that the instantaneous pulse probability is indeterminate. Therefore, Equations 4 and are solved for P as a function of V .

$$P = \bar{P}_0 - \frac{1}{\zeta} \ln \frac{1-V}{V\zeta} \quad P > \bar{P}_0, V < 0 \quad 15.$$

$$P = \bar{P}_0 - \frac{r_d}{\zeta} \ln \frac{1-V}{r_d V \zeta} \quad P < \bar{P}_0, V > 0 \quad 16.$$

From unpublished theoretical results, which lie beyond the scope of this limited review, the value for r is 2.0, so Equations 8 and 14 are modified accordingly:

$$P = P_0 e^{2V} \quad V \leq 0 \quad 17.$$

$$P = P_0(3 - 2e^{-V}) \quad V \geq 0 \quad 18.$$

The value for P_0 (as an estimator for T_0) conforms to the mean pulse rate for each neuron (the total number of pulses divided by the number of thousands of observations), so that only a single unspecified variable, ζ , suffices to fit the theoretical curves to experimental data (Figure 1, upper left).

For any neuron, one of three conditions is assumed to hold. If the limits on (V-P) conversion are dominant, then the asymptotes for $P(A)$ must be horizontal, because at some high positive or negative values of amplitude the pulse probability does not change. If the limits on (P-V) conversion dominate the neuron, the asymptotes are vertical, because excessive values for pulse probability are required to yield wave amplitudes nearing the asymptotic limit. If the limits on the input function are well within the limits for both conversions, then the relationship between P and V is linear or nearly so. Equations 17 and 18 apply to the first case (V-P), Equations 15 and 16 to the second (P-V), and either pair to the third.

Examples of each type of curve are shown in Figure 1, upper row. The pattern for $\hat{P}_m(A)$ reflects (V-P) conversion. That for $\hat{P}_B(A)$ reflects (P-V) conversion. The linear curves for $\hat{P}_A(A)$ are fitted with a curve $P(A)$ from (V-P) conversion, as the converse of $\hat{P}_B(A)$ for the same neural mass.

HOW IS FORWARD GAIN CALCULATED?

The conversion rate for each stage is given by the slope of the input-output curve for each stage, respectively, for curves from Equations 15-16 and 17-18. For each neuron population having two stages it is the product of the two derivatives. The forward gain is denoted K_i^{*5} for inhibition by an inhibitory neural mass and disexcitation by an excitatory neural mass. The forward gain is K_e^{*5} for excitation by an excitatory neural mass and disinhibition by an inhibitory neural mass.

$$K_i^{*5} = - \frac{dP}{dV} \frac{dV}{dP} \quad V < 0 \quad 19.$$

$$K_e^{*5} = - \frac{dP}{dV} \frac{dV}{dP} \quad V > 0 \quad 20.$$

The derivatives of Equations 17 and 18 are

$$\frac{dP}{dV} = 2\gamma \bar{P}_0 e^{2\gamma V} \quad V < 0 \quad 21.$$

$$\frac{dP}{dV} = 2\gamma \bar{P}_0 e^{-\gamma V} \quad V > 0 \quad 22.$$

From the derivations of Equations 15 and 16, we have

$$\frac{dV}{dP} = \zeta(V_i - V) \quad V < 0 \quad 23.$$

$$\frac{dV}{dP} = \zeta(V_i + V/r_d) \quad V > 0 \quad 24.$$

Therefore

$$K_i = -2\gamma \bar{P}_0 \zeta (V_i - V) e^{2\gamma V} \quad V < 0 \quad 25.$$

$$K_e = -2\gamma \bar{P}_0 \zeta (V_i + V/r_d) e^{-\gamma V} \quad V > 0 \quad 26.$$

The "reference gain" is K_0 at $V = 0$.

$$K_0 = -2\gamma \bar{P}_0 \zeta V_i \quad V = 0 \quad 27.$$

Some representative values of the coefficients are as follows (56). The mean value of P_0 for 22 bulbar mitral and tufted cells is 10.1 pps and the mean value for γ_m is .00512/ μ V. For 10 type A neurons the mean for P_0 is 13.8 pps and that for γ_A is .00169/ μ V (5 7). In addition to P_0 (9.6 pps for 12 type B units), three coefficients are evaluated from fitting $P_B(A)$ to $\hat{P}_B(A)$. The mean for r_d is 5.7. The mean for V_i is -138μ V or -3.09σ , slightly lower than three standard deviations of EEG amplitude. The mean for the rate constant ζ_B is 0.41/pps.

The estimated gain factor for (V-P) conversion of mitral-tufted cells is $2\gamma_M P_0 = .10$ pps/ μ V. That for (V-P) conversion type A neurons is $2\gamma_A P_0 = .046$ / μ V. That for (P-V) conversion from type B pulses to type A waves is $-\zeta_B V_i = 56$ pps/ μ V. The estimated value for K_0 for the product of (P-V) and (V-P) conversion factors for superficial pyramidal cells (A) is 2.6. The factor for (P-V) conversion in the bulbar relay can not be estimated because bulbar-granule cells do not generate detectable action potentials.

These numerical estimates are without confidence intervals, particularly in regard to the use of the mean for observed values of P_0 as an estimator of the mean T_0 . There is some bias in the experimenter toward selecting relatively fast-firing neurons for statistical analysis, because they give smoother pictures at lower cost, so that the estimate of the type A forward gain based on T_0 is probably about two-fold too high. The point is that conversion factors and forward gains can be defined by theory and measured by experiment for neural masses. Confidence limits can be established only by extensive experimental follow-up and further molding of the theoretical infrastructure.

Equations 25-27 imply that there is a central quasi-linear amplitude range, in which forward gain is maximal. With increasing positive (excitatory) amplitudes both stages undergo progressive saturation, the (V-P) stage exponentially and the (P-V) stage linearly. With decreasing negative (inhibitory) amplitudes, the (V-P) stage saturates twice as rapidly in the exponential mode and the (P-V) stage six times as rapidly in the linear mode on the inhibitory side as on the excitatory side. The forward gain appears to depend on four parameters or system variables; the population mean pulse rate P_0 ; the ambient maintained degree of depolarization V_i ; and the two rate constants γ and ζ for which an interpretation at the cellular level has not been attempted. Whether these four system variables are or are not independent of each other has not been determined.

WHAT IS THE OPEN-LOOP RESPONSE?

Neurons in masses are densely interconnected by countless numbers of synapses. Normally these are capable of transmitting output depending on the magnitude of input, so that electrical stimulation of a nerve or tract leading to a neural mass leads to multiple sequential synaptically transmitted events in the mass. Repetitive excitation and inhibition of the initially excited or inhibited neurons is the rule. However, by pharmacological means it is feasible to reduce the transmission effectiveness of synapses in the mass, to the extent that background EEG and pulse trains are totally suppressed. In this state the afferent volley, electrically induced, activates the dendrites of neurons at the first synapse, and perhaps the second, but no further. Feedback interaction is reduced to zero, and only forward transmission to the first one or two subsets of neurons in the mass is present. This is referred to as the open-loop state (36, 37).

The experimental proof of this state depends on demonstrating the absence of background unit activity and all but one brief volley of induced firing, if any (37). (This is another example of the manner in which the conjoint recording of pulse and wave activity is essential to the analysis of neural masses.) The averaged dendritic response manifested as the

AEP is the open-loop impulse response of a neural mass.

An example of the open-loop AEP of the olfactory bulb is shown in Figure 2 (top) as the sets of triangles. The response is induced by stimulation of the axons of the mitral cells in the lateral olfactory tract (LOT) antidromically. The volley is delivered by the mitral cells to the granule cells, and the dendrites on synaptic activation generate the field potential yielding the AEP. There is no further transmitted event. A virtually identical open-loop response occurs in the olfactory cortex, generated by the type A neurons in response to an orthodromic LOT volley (34, 38, 57).

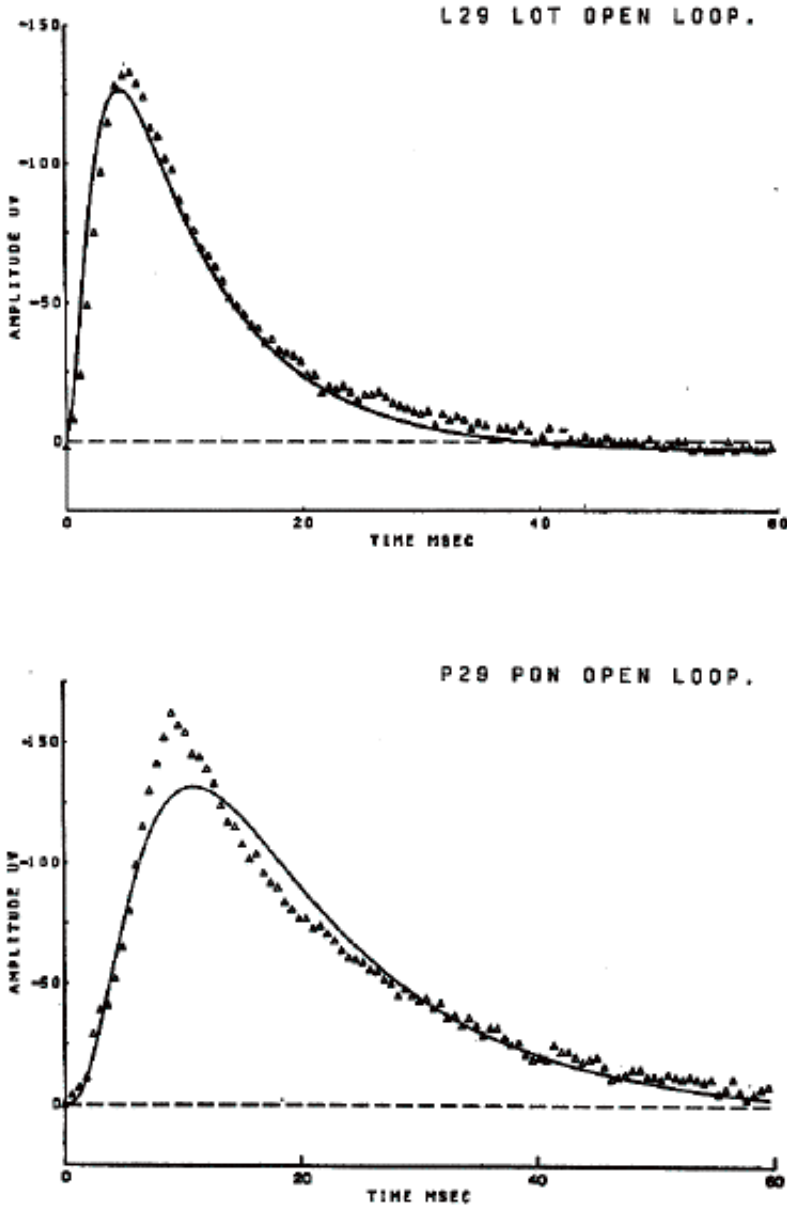


FIGURE 2. These are open-loop responses of bulbar neurons on antidromic LOT (above) or orthodromic PON (below) single-shock electrical stimulation. AEPs (triangles) $N=100$. Curves are from the inverse transforms of Equation 28 (above) and of Equation 30 (below).

In essence³ these experimental data have been fitted by the sum of three exponentials:

$$a(t) = \sum_{i=1}^3 A_i e^{-a_i t} \quad 28.$$

where a_1 is the rate constant of the decay of the response, a_2 is that of the rising phase, and a_3 is that determining the curvature of the foot of the response. The Laplace transform of Equation 29 gives the differential equation for the dendritic open-loop response:

$$A(s) = A_0 \prod_{i=1}^3 \left(\frac{a_i}{s + a_i} \right) \quad 29.$$

³[The experimental determination of the open-loop rate constants is complicated by the presence of dispersion in afferent axonal pathways, which is not part of the delays found within the loops of the neural mass. For LOT input to the bulb and cortex, this dispersion $A_x(s)$ is negligible, but for PON input it is rather strong (47). Therefore, the total transference for PON input is $A(s)A(s)A(s)$. The forward transference within the bulb is

$A(s)A(s)$. The separation of $A_x(s)$ from $A_m(s)$ requires measurements in both open- and closed-loop states, using both orthodromic (forward limb) and antidromic (feedback limb) inputs.

A simple experimental test to determine whether $A_x(s)$ can be ignored is to search for the afferent axonal or cell body compound action potential in the mass preceding the dendritic response. If it cannot be detected (other than in the form of intracellular or extracellular unit potentials), then it has been degraded by temporal dispersion acting as a low pass filter (47), and $A_x(s)$ must be explicitly evaluated in order to evaluate $A(s)$ with adequate precision.]

Mean values for the rate constants are $a_1 = 220/\text{sec}$ (equivalent to a time constant of 4.55 msec), $a_2 = 720/\text{sec}$ (1.38 msec), and $a_3 = 2300/\text{sec}$ (0.43 msec).

The similarity of these rate constants to those computed from intracellular measurements on single cells (49, 58-62) bulbar measurements on single cells (49, 58-62) strongly suggests that a , can be taken to represent mainly the passive membrane RC decay rate, a_2 the lumped synaptic and cable delays (both equivalent to one-dimensional diffusion processes), and as the effect of axonal delays within the mass, which are very short (37). However, the rate constants of the mass cannot be uniquely identified with these known sources of delay in single neurons on a one-to-one basis.

This procedure to identify and measure the rate constants (and to interpret them in terms of underlying processes) is formally identical to that used to define "passive" membrane resistance and capacitance (59). For an axon or a group of axons a range of response amplitudes is defined over which additivity and proportionality hold. Within this range the response in membrane potential $v(t)$ to a current step I . $U(t)$ is recorded. It is fitted with a rising exponential curve having the equation $v(t) = k \cdot I \cdot U(t) \cdot (1 - e^{-t/\tau})$ where $r = 1/a$ is the time constant in sec and k is in units of ohms and depends on the value for the potential as $t \rightarrow \infty$. The Laplace transform is $V(s) = I \cdot k / (s\tau + 1)$. The transfer function is the ratio of the transforms of the input and output functions, $V(s)/I(s) = k / (s\tau + 1)$. A differential equation is then written to describe the discharge of a capacitor C through a resistor R after C has been charged by a current pulse $I \cdot \delta(t)$. This can be written $Cdv(t)/dt = I \cdot \delta(t) - v(t)/R$. The Laplace transform is $V(s)/I = R / (sRC + 1)$. It is next inferred that $R = k$ and $C = \tau/k$. Numerical estimates for R and C are then obtained in a variety of experimental conditions to confirm the dynamic range of linearity for the preparation, which is the range of validity for the differential equation and its evaluated coefficients.

It is well known that both R and C of biological membranes vary with frequency (60), but the approximation of their behavior within the usual experimental range of function to ohmic resistance and coulombic capacitance is close enough for most purposes. Moreover, each is an average measurement over a large ensemble of membrane structures, such as the sodium or potassium channels, which on more intensive analysis outside the linear range are identified and measured by elaborate equations, e.g., the Hodgkin-Huxley equations (61). Or the linear model is retained but the lumped circuit approximation is dropped, and the spatial dimensions are introduced, e.g., in the form of a cylinder (8, 62) or a branching dendritic tree (8, 9, 63).

In all these cases the response waveform for a severely limited input guides the selection of an appropriate set of linear basis functions and the construction of a linear differential equation. The equation is modified and elaborated to extend prediction and observation into a broader functional range. The essential difference in the present usage is that linear equations are used to describe and measure the properties of the neural mass, and the interpretation of the results is directed toward known components at the next lower level of complexity, that is, the properties of neurons rather than the properties of membranes.

On the other hand the same results are used as the basis for interpretation of the next highest level of complexity. An immediate example of neural masses is the AEP response of the bulbar granule cells $A(s)$ to excitation of the primary olfactory nerve (PON), shown in Figure 2 (bottom). The afferent volley is transmitted orthodromically through the mitral-tufted cell pool having the transference $A_m(s)$. It is found experimentally (W. J. Freeman, unpublished results) that $A_m(s)$ is almost identical to $A(s)$, so that the overall transfer function for the two neural masses in series, $A_g(s)$, is

$$A_g(s) = A^2(s) \quad 30.$$

The inverse transform of Equation 30, which contains double poles after substitution of Equation 29, is too cumbersome to reproduce here. The predicted waveform is shown as the curve in Figure 2 (bottom). The interpretation at the first sublevel is that the delays introduced by the two neural masses in series are about equal to each other, and at the second sublevel that the passive membrane decay rates for the mitral-tufted and granule cells are equal, despite the gross differences between virtually all other properties of the two cell types. These same rate constants and interpretations hold for types A and B neurons in the cortex as well (34, 36, 37, 48).

WHAT ARE THE CHARACTERISTICS OF NEGATIVE FEEDBACK?

The mitral and tufted cells in the bulb (type M) are excitatory, whereas the granule cells (type G) are inhibitory. Excitation of type M cells by single-shock stimulation normally leads to excitation of type G cells and to feedback inhibition of type M cells (46). The inhibited type M cells disexcite type G cells which disinhibit or re-excite type M cells, and so on, such that the impulse response in the closed-loop state is predictably oscillatory. The same prediction holds for

the interaction of types A and B neutrons in the cortex (34, 36, 57).

In a narrowly limited range of function (to be described in a later section), the transfer function for these negative feedback loops for orthodromic input to the excitatory neural mass and output (Figure 3, upper right) from the same neural mass (the forward limb) is

$$C_{ee}(s) = \frac{A(s)}{1 + K_n A^2(s)} \quad 31.$$

For input to the forward limb and output (Figure 3, lower right) from the feedback limb (the inhibitory bulbar or cortical granule cells), the transference is

$$C_{ei}(s) = \frac{A^2(s)}{1 + K_n A^2(s)} \quad 32.$$

For antidromic input to the feedback limb and output from the forward limb (Figure 3, upper left) or output from the feedback limb (Figure 3, lower left) the transfer functions are respectively

$$C_{ie}(s) = \frac{C_{ee}(s)}{A(s)} \quad 33.$$

$$C_{ii}(s) = \frac{C_{ei}(s)}{A(s)} \quad 34.$$

In each of Equations (31-34) the feedback gain is $K_n = (K_e K_i)^{.5}$, where $K_e^{.5}$ and $K_i^{.5}$ are defined by Equations 19 and 20.

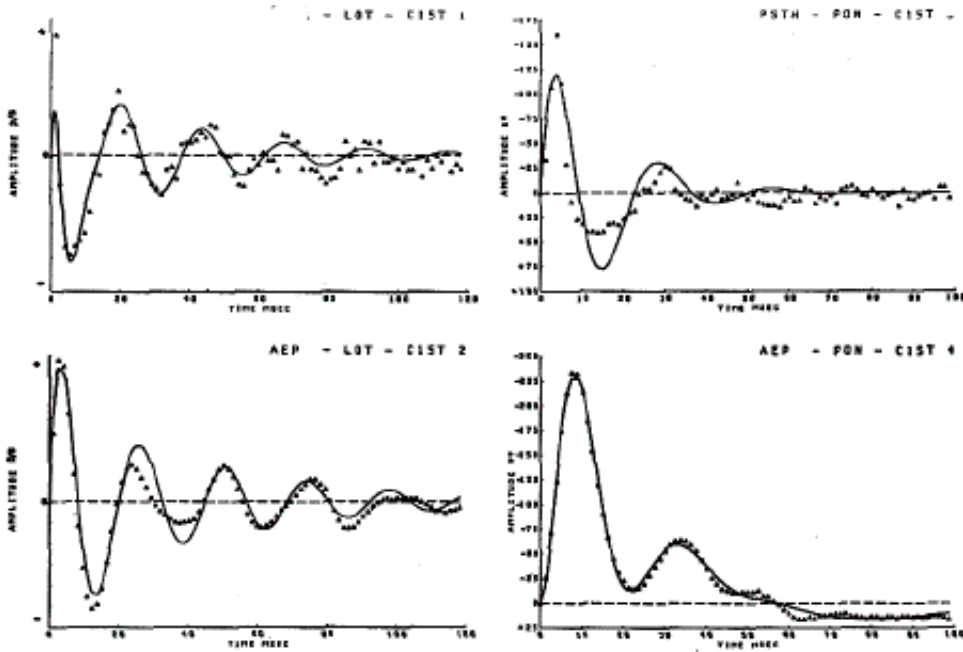


FIGURE 3. PST histograms (above) of a single mitral cell and AEPs (below) of granule cells upon LOT (left) or PON (right) stimulation are fitted with curves for predicted responses from Equation 35 (closed loop, negative feedback). There is phase lag of the AEP from the PST histogram of about one quarter cycle (see Figure 1, lower left). Transfer functions: upper right, Equation 31; lower right, Equation 32; upper left, Equation 33; lower left, Equation 34.

Following substitution of Equation 29 into any of Equations 31-34, factoring of the denominator, and partial fraction expansion, the inverse Lapace transform yields the equation for a damped sine wave with a sigmoidal inflection at the foot of the first upward peak (34, 36, 48):

$$c(t) = \sum_{i=1}^n V_i \sin(\omega_i t + \phi_i) e^{-\alpha_i t} \quad 35.$$

The same equation holds for predictions of the state variables of both forward and feedback limbs. The frequencies and decay rates are identical, but the phase of the feedback limb transient characteristically displays a quarter cycle phase lag from that of the forward limb transient.

These predicted transients are shown as curves in Figure 3 fitted to the PST histogram (triangles, above) of a mitral cell (excitatory, forward limb) and to the AEP (triangles, below) of the granule cells (inhibitory, feedback limb). The common frequency and decay rate are apparent, as well as the phase lag of each AEP from the corresponding PST histogram (48).

The bulbar responses to PON stimulation (Figure 3, right), which is orthodromic and to the forward limb, show approximately one quarter cycle phase lag over the bulbar responses to LOT stimulation (Figure 3, left), which is antidromic and to the feedback limb, as predicted by Equations 31-34.

The comparison of AEPs generated by type A neurons in the cortex (37) on orthodromic (LOT) stimulation with PST histograms shows that the AEP is in phase with the oscillation in PST histograms from type A neurons (forward limb) and leads the oscillation in PST histograms for type B neurons (feedback limb) by about one quarter cycle. These same phase relationships are shown in Figure 1 (lower row) for background pulse and wave activity.

The mean value for K_n , obtained from the Laplace transform of Equation 35 after fitting curves to the AEPs and PST histograms for both bulb and cortex, is between 1.75 and 2.25 (36). The value for K_n , representing effective connection density within the mass, is a property only of the mass and not of the single neurons in the mass. The measured values for the rate constants are the same in the open-loop and closed-loop states. These and related results (36, 37) imply that the rate constants can be treated as invariants, and that the amplitude-dependent nonlinearity $P(V)$ can be introduced into the linear equations $C(s)$ as a variable gain coefficient.

WHAT ARE THE CHARACTERISTICS OF POSITIVE FEEDBACK?

The example given for negative feedback is based on the assumption that a neural mass contains large numbers of excitatory and inhibitory neurons having reciprocal connections. If the mass contains excitatory neurons maintaining significant feedback connections with each other, a different kind of feedback loop must be considered. This is a positive feedback loop, in which excitatory neurons excite and re-excite each other in the mass upon initial excitation. The pattern is familiar among physiologists as "avalanche conduction" or the "reverberating circuit."

Such loops usually appear in neural masses having negative feedback as well, and seldom occur in isolation. An example of the latter is to be found in the periglomerular neurons of the olfactory bulb (40, 41, 45, 48). An illustration of the impulse response of one of these neurons is shown in Figure 4, left. The three sets of triangles illustrate three PST histograms at low, medium, and high PON stimulus intensity. (The background pulse rate of the neuron, which is constant, is indicated by the height of the baseline above the abscissa. This gives the change in scale from which to measure the increase in pulse rate at the crest of the response with increasing stimulus intensity.)

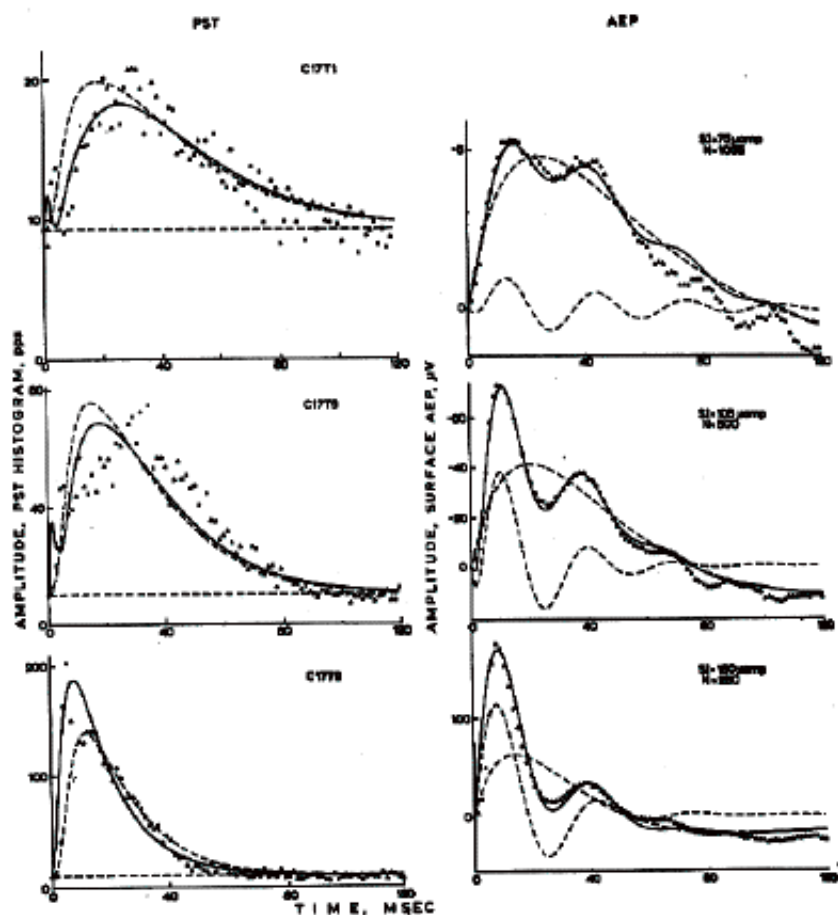


FIGURE 4 (from Freeman 48). Left. The PST histograms (triangles) of pulses from a single periglomerular neuron represent the output of a neural mass having internal positive feedback. The lowest rate constant increases with increasing response amplitude. The change in scale for display of the histograms is reflected in the decreased scale for the constant background activity (Equation 37).

Right. AEPs from the bulbar granule cells (concomitantly recorded field potential) show the granule cell response to the PON impulse input (the oscillatory component) and to the periglomerular cell input (the monotonic component). Initial response amplitudes: 22 μV , 324 μV , 986 μV (Equations 35 and 37).

In qualitative terms the response of the neural mass to an impulse input by way of the PON is a rapid increase in mean pulse rate above the baseline of background activity, which then decays with a slow rate constant. When the input intensity is increased, the induced pulse rate is augmented, but so also is the decay rate of the response. There is no terminal overshoot.

The response of this neural mass cannot be directly detected in the form of an extracellular field potential. The concomitantly recorded AEPs shown in Figure 4 (right) display a sinusoidal oscillation generated by the bulbar negative feedback loop, to which both the PON and the periglomerular neurons project. The oscillation is superimposed on a monotonic shift in baseline, which is the granule cell response to periglomerular input. It is not owing to a field potential of periglomerular cells.

The dynamics of this neural mass can be described in terms of a positive-feedback loop, having input to a subset (B_1) of the periglomerular cells constituting the forward limb, interacting with another subset (B_2) of the same mass not receiving the initial impulse input and constituting the feedback limb. The transfer function for output from the forward limb is

$$B_1(s) = \frac{A_0 \cdot A(s)}{1 - K_p A^2(s)} \quad 36.$$

where $A(s)$ is defined in Equation 29 and $K_p = K_e$, is the square of excitatory forward gain defined by Equation 20; A_0 is a forward gain constant.

After substituting Equation 29 into Equation 36, reducing fractions, and expanding the denominator in partial fractions, the inverse Laplace transform yields

$$b_1(t) = \sum_{j=1} B_j e^{-b_j t} + B_3 \cos(\omega t + \phi) e^{-b_3 t} \quad 37.$$

where the amplitude coefficients B_j and B_3 depend on the open loop rate constants a_j , the feedback gain K_e , and a forward gain constant A_0 .

The rate constants⁴ are invariant with stimulus intensity at the values $a_1 = 230/\text{sec}$, $a_2 = 550/\text{sec}$, and $a_3 = 2300/\text{sec}$. The value for A_0 increases in proportion to stimulus magnitude. The change in the closed-loop rate constants, most notably that for the decay rate of the response b_1 , is owing solely to the change in K_e predicted by Equation 26, where either A_0 or B_1 or the crest amplitude of the PST histogram is used to estimate V .

⁴ [Owing to the inaccessibility of a dendritic field potential from those neurons, the open-loop rate constants were determined by trial and error. A sum of exponential curves and a damped sine wave (Equation 37) was fitted to the data (Figure 4, left, solid curves, and Figure 5, open triangles). The transfer functions for $A_x(s)$ and $A(s)$ were evaluated by initial guesses, and root locus plots were calculated. When optimal values for the open-loop poles had been found, the results were checked by generating new curves using these invariants (Figure 4, left, dashed curves). The neural mass was found to have the same rate constants as the other masses in the bulb and cortex, within the limits of experimental error (34).

This case illustrates a general principle in the analysis of neural dynamics, that sets of AEPs and PST histograms, taken in conjunction with systematic variation of an antecedent variable, can be used to compensate for the limitations imposed by the inaccessibility of some of the state variables of neural masses to direct measurement.]

These and related results (36, 48) show that positive feedback among neurons in masses leads to monotonic responses with decay rates that are not the same as those of the component neurons. The rate constants of the neural mass with internal positive feedback have much lower values than those usually assigned to passive membrane. Furthermore, whereas by inference the rate constants of the component neurons in the mass are invariant with respect to response amplitude over the designated range of observation, the rate constants of the neural mass are amplitude-dependent, primarily owing to the presence of saturation in the feedback path.

This type of long-lasting neural response has been observed to follow electrical stimulation in many parts of the nervous system, most prominently in the spinal cord (64, 65), where the prolonged impulse responses have been associated with presynaptic inhibition. However, the dependencies of the rate constants on response amplitudes have not been measured with adequate precision, and the associations with concomitantly recorded PST histograms have not been well enough established, to permit strong inference that these responses manifest positive excitatory feedback, although it seems likely that many of them do.

Mutual inhibition can be modeled using Equations 36 and 37. An example is the lateral eye of *Limulus* (19), which consists of an array of about 101 densely interconnected receptor neurons having a common input (light) and a common sign of output (inhibition). They form a positive inhibitory-feedback loop in which the gain characteristic is linear over a certain range but is bounded by saturation (threshold) on the inhibitory side. Above that level the function is readily approximated by linear analysis (20).

A similarly isolated example of an inhibitory neural mass has not been identified in the mammalian nervous system.

Inhibitory neurons seem always to be densely connected with excitatory neurons as well as with each other. Therefore, information about them is indirect. Their predicted patterns of behavior correspond to those for excitatory interactions in most aspects. But whereas the outputs for the forward and feedback limbs of an excitatory neural mass during the impulse response both increase and decrease together, in the inhibitory neural mass they change in opposite directions. On initial excitation, for example, the activity of the forward limb increases, which inhibits the activity of the feedback limb. The latter disinhibits or further excites the forward limb, which further inhibits the feedback limb. The time courses of the two parts are parallel and monotonic, but have opposite polarity.

WHY USE ROOT LOCUS DISPLAY?

The dynamic relation between the rate constants of the closed-loop response and the underlying physiological variable, the closed-loop gain, is best displayed by a root locus representation in the s plane (29, 35). Such a diagram is shown in Figure 5 for Equation 36, which on substitution of Equation 29 and reduction of fractions becomes

$$B_1(s) = \frac{\prod_{i=1}^3 (s + a_i)}{\prod_{i=1}^3 (s + a_i)^2 - K_e a_1^2 a_2^2 a_3^2} \quad 38.$$

On expansion and factoring of the polynomial in the denominator, this becomes

$$B_1(s) = \frac{\prod_{i=1}^3 (s + a_i)}{\prod_{j=1}^6 (s + b_j)} \quad 39.$$

where the closed-loop rate constants b_j are determined by the open-loop rate constants a_i and K_e . The closed-loop zeroes at $s = -a_1$ and $s = -a_2$ appear as open squares on the negative real axis in Figure 5, at the locations of the open-loop poles. The poles and zeroes at $s = -a_3$ are far to the left. Experimental closed-loop roots appear as the four sets of triangles where the four loci intersect representative gain contours between $K_e = 0.53$ and 0.19. For each value of K_e there are four real roots and two complex roots. The latter predict the overdamped cosine component in the rise of the output. The rate constant specified by the pole b_1 nearest the $j\omega$ axis determines the decay rate of the impulse response.

The method displays in a single graph the open-loop rate constants (which are invariant), the closed-loop rate constants, the ambient level of gain (which is amplitude-dependent), and the predicted change in the impulse response with changes in amplitude or other determinant of gain. Also shown are the locations of the closed-loop zeroes, which play an important role in precision analysis, and the stability characteristics of both real and model systems.

The technique is especially well adapted for use in conjunction with impulse stimulation. Owing to the fact that direct access to most neural masses in the brain is by nerves and tracts, which are accessible only to electrical pulses, the impulse response (the AEP and the PST histogram) is the most common source of information on their active states.

The curve fitted to each impulse response yields coefficients, which form a constellation of poles and zeroes in the s plane. Many physiological variables, but particularly response amplitude variation, generate successive values for the coefficients, which define sets of "physiological" root loci as indicated by the triangles in Figure 5. These loci are matched by theoretical root loci, which are generated from differential equations based on the topology of connections and the open-loop rate constants of the neurons. They serve to evaluate the closed-loop gain.

The ultimate justification for reliance on the root locus diagram (29) as a basic analytic tool in neural dynamics is the feasibility of separation of the transference into a linear frequency-dependent part and a nonlinear amplitude-dependent part, the former evaluated by fixed rate constants and the latter by variable gain coefficients. No other method of system representation seems so well adapted to this feature of neural masses.

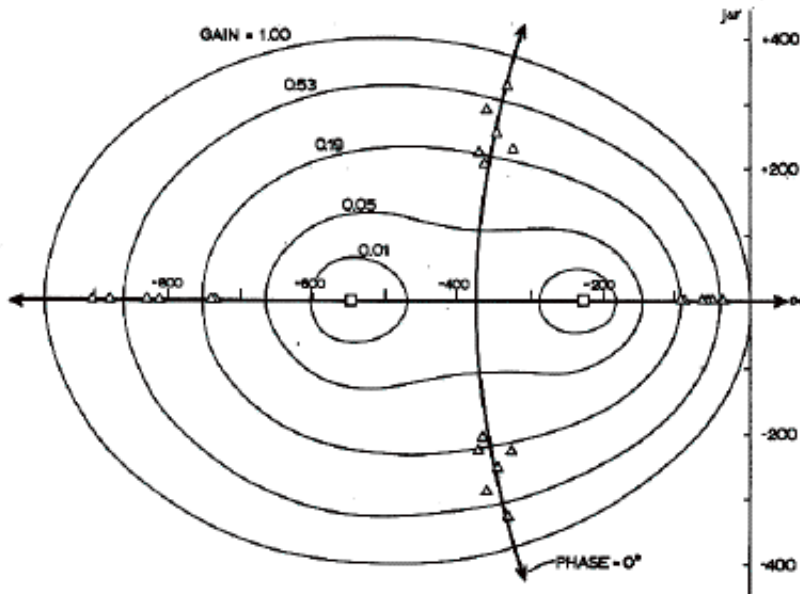


FIGURE 5. This is a root locus diagram in the s plane for neural positive feedback. The triangles show the rate constants of the solid curves in Figure 4 (left). The open squares show the locations of the open-loop poles and closed-loop zeroes. The solid curves are the root loci. The light curves are representative gain contours.

WHAT ARE THE CHARACTERISTICS OF MULTIPLE-LOOP FEEDBACK?

Doubtless the most common neural mass by far is the mixture of excitatory and inhibitory neurons, which are densely interconnected with each other without restriction as to cell type. The minimum topology of such a mass contains multiple loops of three kinds: negative, positive-excitatory, and positive-inhibitory feedback (36). Three feedback gain coefficients are required: K_e , K_i , and K_n .

A twelfth-order differential equation is required to represent the connections of such a neural mass, in which the open-loop transference of the subsets composing it, $A(s)$, is specified and evaluated by Equation 29 and in the text following. The techniques for formulating and solving the equation have been given elsewhere (36, 57). The solution for the impulse response predicts a damped sine wave in the output, which is superimposed on a monotonic transient (similar to that in Figure 4, right). The oscillation is due to the negative feedback loop, and the monotonic transient is the output of whichever of the two positive feedback loops has the higher gain.

Changing the intensity of the stimulus delivered to a mixed neural mass characteristically alters the frequency ω and decay rate α of its oscillatory response (36-39). Measurement of the series of AEPs such as that shown in Figure 4, right, yields sets of values for ω and α that in the s plane define a physiological root locus for the neural mass with changing input intensity (Figure 5, circles). The frequency is characteristically reduced and the decay rate is augmented with increased input magnitude. The changes imply, in accordance with Equations 25 and 26, that the feedback gains are reduced with increasing amplitude owing to saturation.

Calculations to fit these physiological root loci are complicated by two factors. First, all three gain coefficients must be expressed as dependents on one variable (input or response amplitude, which has both positive and negative extremes). Second, the input to the mass may consist not merely of an impulse, but of a prolonged monotonic input function, such as that from periglomerular neurons to mitral and bulbar granule cells (Figure 4). The degrees of saturation on the excitatory and inhibitory sides and their ratio may vary widely, depending on the magnitude of this baseline shift.

An interim technique to achieve the calculation is based on the use of an empirical dimensionless factor 5, which serves to define the dependence of K_e and K_i on K_n :

$$K_e = K_n \left(\frac{K_n}{K_0} \right)^5 \quad 40.$$

$$K_i = K_n \left(\frac{K_n}{K_0} \right)^{-4} \quad 41.$$

where K_0 is a reference gain (see Equation 27) at which $K_n = K_e = K_i$. When this condition holds (even for $\partial \neq 0$), the mixed neural mass is reduced to a single negative-feedback loop, so that K_0 has a value between 1.75 and 2.25.

From the product of the left-hand terms of Equations 40 and 41 set equal to the product of the right-hand terms, $K = (K_e K_i)^5$.

It is found empirically (W. J. Freeman, unpublished data) that the locus for a neural mass with an impulse input is replicated by a value for $\partial = -0.5$. For a mass with an excitatory monotonic function or bias in the input, ∂ approaches zero. This serves to describe the bulbar physiological root locus for PON input. For an inhibitory bias, ∂ approaches -1 . The latter value serves to describe the physiological root locus of the olfactory cortex for LOT input (36, 39).

These characteristic curves for neural masses are shown as a family in Figure 6 for a value of $K_o = 2.24$. The curvilinear segments from upper left to lower right designate values for gain expressed as the $\log_{10}(K_n K_o)$. The stability limits to the left of the $j\omega$ axis (at the high-frequency, low-amplitude, high-gain ends of the curves) are determined by a root locus (not shown) on the real axis of the s plane, which crosses the $j\omega$ axis to the right with decreasing amplitude. The stability characteristics at the low-frequency, high-amplitude ends of the curves have been discussed elsewhere (36). The characteristic curves are used as follows. The open-loop rate constants are determined for a neural mass. Then in some normal physiological state a set of AEPs over a range of stimulus intensities is obtained and measured. The frequencies and decay rates define the physiological root locus. The position and orientation of the locus serve to evaluate K_o and ∂ . The values for α and ω serve to evaluate K_n . Equations 40 and 41 evaluate K_e and K_i . By this means the closed-loop responses suffice to specify the three feedback gains (functional connection densities) in the mass. The logarithms of the gains (with reference gain at K_o) are plotted as a function of the amplitude of the oscillatory component of the impulse response to determine conformance of the dynamics of the mass to the type of saturation predicted by Equations 25-27. The value for ∂ serves to predict the sign and magnitude of the monotonic component of the impulse response (Figure 4, right).

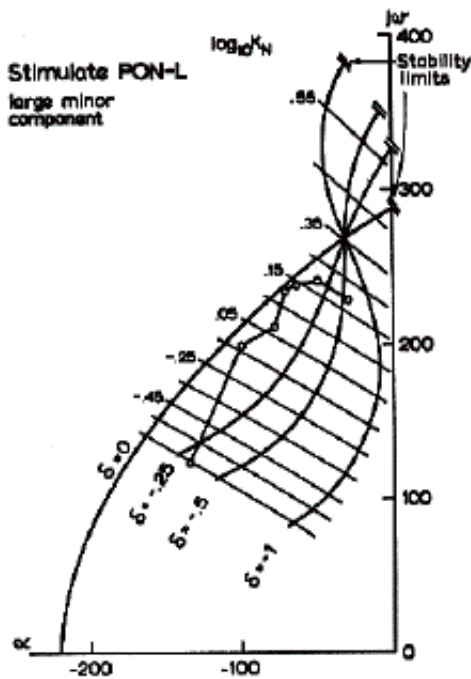


FIGURE 6. This is a composite diagram of four root loci in the upper left quadrant of the s plane. Each heavy curve is a locus for a single complex pole. Open circles are from an experimental set of AEPs, some of which are reproduced in Figure 4, right. With increased stimulus intensity the AEP frequency and the gain K_n both decrease. Corresponding values for K_n are connected by light arcs. For a single negative-feedback loop, $\partial = 0$. For both negative and positive feedback with an impulse input, $\partial = -.5$. For an impulse input superimposed on an excitatory bias to a mass having both positive and negative feedback (Figure 4, right), $\partial > -.5$. For inhibitory bias, $\partial < -.5$. The normal midrange operating condition for the olfactory neural masses (Figure 3) appears to be ∂ near $-.5$ and K_n near 2.24 ($\log_{10} K_o = 0.35$). The open loop double pole (Figure 2) is at $s = -220/\text{sec}$. Root loci on the negative real axis (as in Figure 5) are not shown here.

An interesting alternative approach to the description of this multiple-loop neural configuration has been developed by Wilson & Cowan (66). They derived coupled nonlinear differential equations to predict the responses of a neural mass having negative feedback and the two kinds of positive feedback. A single rate constant was used for the delay $[A(s), i=1]$, and the logistic curve was used to represent the input-output curve (Figure 1). Using phase-plane methods and numerical integration, they found multiple stable states as well as limit-cycle oscillation, corresponding to the real and complex roots of Equations 35 and 37. The frequency of oscillation was also found to be a monotonic increasing function of stimulus intensity.

The intensity referred to in their model is the sustained input to either or both subpopulations, which is equivalent here to a background bias maintaining the mean activity level V_o at some level other than zero. As the bias is increased their limit-cycle frequency goes monotonically from some minimum to some maximum value, above which the oscillation is

suppressed. Experimentally (38), in bulb or cortex the bias can be increased by use of tetanizing electrical stimulus pulse trains or decreased by administration of pentobarbital or other anesthetic. The frequency changes in the predicted manner (cf. Figure 12a in 66 and Figure 2 in 38). The characteristic curves shown in Figure 6 ($\partial \leq .5$) hold equally for increasing bias or for decreasing test pulse intensity (39). That is, frequency is determined by the ratio of test pulse to bias amplitude, not by either alone.

The Wilson-Cowan model displays some remarkable hysteresis properties not apparent from linear analysis. On the other hand the replication of the observed "physiological" root loci with calculated root loci (36, 39) could not be achieved unless the approximation for the open-loop response contained at least three poles [$A(s)$, $i=3$]. It is unlikely that phase-plane methods can readily be adapted to twelfth-order systems, to provide the means for identification and measurement of experimental observations. Each approach has its advantages and the interaction between linear and nonlinear analysis is bound to be fruitful.

HOW WIDELY MIGHT THESE TECHNIQUES BE APPLIED?

AEPs often seem complex in appearance, particularly when comparisons are being made between those from different parts of the brain. This is deceptive. When the proper basis functions are used in conjunction with signal detection theory (30, 35), the typical AEP can be measured, stored, and reconstructed using a rather small set of numbers (67). The real complexity of AEPs resides in the sensitivity of their waveforms to a host of experimental factors, including the sites of stimulation and recording, the parameters of the input, the conditions of the animal, and the local state of the neural mass (14, 39, 42-46). When any one of these antecedent variables is changed, several or all of the numerical coefficients of the basis functions change in a coordinated way (39). The patterns of variation reveal more information about the neural mass than do the mean values of the coefficients. This is why root locus techniques combined with factor analysis (39, 67) and analysis of variance (68) of AEP sets are so useful (see footnote 4).

The characteristic curves shown in Figures 5 and 6 and related curves (36) hold for neural masses in the olfactory system over a response amplitude range from several microvolts to several millivolts, and a response frequency range from 0 to 60 Hz and above. It is suggested that any neural mass having characteristic frequencies in this range is likely to have dynamics closely related to those of the olfactory system. These include such structures as the hippocampus (69), the superior colliculus (70), the thalamus (71), and most if not an areas of the neocortex (13, 22, 25, 26, 72, 73). The impulse responses of the hippocampus (69) and superior colliculus (70) have been shown to conform to damped sine waves, for which the frequency decreases with increasing input intensity. The neocortical areas generate EEG waves in the β range (15 to 30 Hz and above). The presence of a β frequency selective system in the visual analyzer has been thoroughly documented by Lopes da Silva and his colleagues (13, 22) from its responses to sine wave input.

The outstanding difficulty in determining whether the characteristic curves in Figures 5 and 6 apply also to these other structures is experimental. The open-loop rate constants must be measured to determine whether the values conform to those used to evaluate $A(s)$. This in turn requires that the transference of the input pathway $A_x(s)$ be specified (see footnote 3). This is not straightforward for neocortical neural masses in terms of electrical stimulation, because the input and output axons are not physically separated as they are in the olfactory system, so that an afferent volley is likely to be mixed orthodromic and antidromic. Even so, it seems feasible and should be attempted. Otherwise the interaction densities (feedback gains) cannot be defined and evaluated.

WHAT IS THE SIGNIFICANCE OF LINEAR ANALYSIS?

The application of linear analysis does not of itself yield a theory of neural masses. It is an empirical tool for observation, description, measurement, and prediction. It provides the basis functions for fitting the AEPs and PST histograms; it helps to define appropriate ranges for the input parameters; it forces consideration of the details of topologies of interconnection; it provides the means for using the values for frequencies and decay rates of responses in differing physiological states to estimate the numerical magnitudes of the interconnections; and it gives an effective framework in which to study the relations between single neural pulse trains and dendritic currents from large masses of cells, both evoked AEPs and "spontaneous" or background EEG.

These features in themselves amply justify further applications of the technique to larger and more complexly organized neural masses. But to what end? Granted that neurons in large numbers undergo correlated changes in activity following natural or artificial stimulation of the nervous system, does the mere fact of correlation justify the conception of a neural mass? Does the covariance of large-scale activity in itself have any significance for behavior, or is it epiphenomenal? Is sensory or perceptual information conveyed in broadly distributed spatio-temporal patterns of covariance among neurons (74-76), or in the pulse trains of single neurons (77-79)? Might the apparent properties of neural masses be significant merely in terms of the large-scale normalizing, scaling, and smoothing functions required for the operations of single neurons, thus providing the "ground" against which the "figure" is inscribed? Are the results of neuro-electrical measurements in the conditions prescribed by linear analysis relevant to any of these possible functions of neural masses? Is it feasible to construct valid theories of neural information processing, storage, and retrieval without prior working knowledge of the properties of neural masses?

These questions cannot be answered yet, primarily because so little is known about the dynamics of neural masses. The results briefly summarized here imply that neural masses do exist in at least an operational sense, that they have properties distinct from those of single neurons, that these reside in poorly understood distributions of firing rates, thresholds, interconnections, etc, and that these properties must be defined and measured in terms of statistical averages of neural activity.

Linear analysis can best serve now to open a door to the experimental study of neural masses, as it did 40 years ago to the study of membranes, axons, and dendrites of single neurons (59). Beyond this there is the expectation that when the essential nonlinearities of neural masses have been clarified, linear and quasi-linear equations will be supplanted by the "real" equations, as the nonlinear Hodgkin-Huxley equations superseded older "two-factor" theories (61) for axon function. However, the axolemma and the neural mass are complex in different ways, primarily in the relative looseness of the coupling among the component parts for the latter. The alternative possibility must be considered seriously that matrices of linear equations may become the basic working tools for the articulation of our knowledge of how brains work. This point serves to emphasize how little we really know about neural masses, and how rich the opportunities are for studies of them in both theoretical and experimental neurophysiology.

LITERATURE CITED

1. Blinkov, S. M., Glezer, I. I. 1968. *The Human Brain in Figures and Tables*. New York: Plenum
2. Bullock, T. H., Horridge, G. 1965. *Structure and Function in the Nervous Systems of Invertebrates*. San Francisco: W. H. Freeman
3. Sholl, D. A. 1956. *The Organization of the Cerebral Cortex*. London: Methuen
4. Coggeshall, R. E. 1967. *J. Neurophysiol.* 30:1288
5. Barlow, R. B., Jr. 1969. *J. Gen. Physiol.* 54:383
6. Eccles, J. C. 1964. *The Physiology of Synapses*. New York: Academic
7. Gardner, E. 1964. *Fundamentals of Neurology*. Philadelphia: Saunders
8. Lorente de Nó, R. 1947. *J. Cell Comp. Physiol.* 29:207
9. Rall, W. 1962. *Ann. NY Acad. Sci.* 96: 1071
10. Horowitz, J. M., Freeman, W. J. 1968. *Bull. Math. Biophys.* 28:519.
11. Freeman, W. J., Patel, H. H. 1968. *Electroencephalogr. Clin. Neurophysiol.* 24:444
12. Plonsey, R. 1969. *Bioelectric Phenomena*, Ch. 5. New York: McGrawHill
13. MacKay, D. M., Ed. 1969. *Neurosci. Res. Progr. Bull.*, Vol. 7, No. 3, Ch. 1, 4. Brookline, Mass.: Neurosci. Res. Progr.
14. Sherrington, C. S. 1906. *The Integrative Action of the Nervous System*. New Haven: Yale Univ. Press
15. Sherrington, C. S. 1929. *Proc. Roy. Soc. London* 105B:332
16. Denny-Brown, D. 1940. *Selected Writings of Sir Charles Sherrington*. New York: Hoeber
17. Granit, R. 1963. *Progr. Brain Res.* 1:23
18. Brookhart, J. M., Kubota, K. 1963. *Progr. Brain Res.* 1:38
19. Hartline, H. K., Ratliff, F. 1958. *J. Gen. Physiol.* 41:1049
20. Knight, B. W., Toyoda, J., Dodge, F. A., Jr. 1970. *J. Gen. Physiol.* 56:421
21. Stark, L., Sherman, P. M. 1957. *J. Neurophysiol.* 20:17
22. Lopes da Silva, F. H., van Rotterdam, A., Storm van Leeuwen, W., Tielen, A. M. 1970. *Electroencephalogr. Clin. Neurophysiol.* 29:260

23. Cleland, B., Enroth-Cugell, C. 1968. *Acta Physiol. Scand.* 68:365
24. Maffei, L. 1968. 1. *Neurophysiol.* 31: 283
25. Regan, D. 1968. *Electroencephalogr. Clin. Neurophysiol.* 25:231
26. Tielen, A. M., Kamp, A., Lopes da Silva, F. H., Reneau, J. P., Storm van Leeuwen, W. 1969. *Electroencephalogr. Clin. Neurophysiol.* 26:381
27. Freeman, W. J. 1962. *Exp. Neurol.* 5: 477
28. Freeman, W. J. 1963. *Int. Rev. Neurobiol.* 5:53
29. Harris, L. D. 1961. *Introduction to Feedback Systems.* New York: Wiley
30. Huggins, W. H. 1960. Johns Hopkins Univ. Report No. AFCRC-TN-60360
31. Freeman, W. J. 1964. *Exp. Neurol.* 10: 475
32. Hermann, H. T., Stark, L. 1963. *J. Neurophysiol.* 26:215
33. Houk, J., Simon, W. 1967. 1. *Neurophysiol.* 30:1466
34. Biedenbach, M. A., Freeman, W. J. 1965. *Exp. Neurol.* 11:400
35. Smith, O. J. M. 1958. *Feedback Control Systems.* New York: McGrawHill
36. Freeman, W. J. 1967. *Logistics Rev.* 3:5
37. Freeman, W. J. 1968. *J. Neurophysiol.* 31:337
38. Ibid. 349
39. Ibid. 1
40. Ramon LAMBDA Cajal, S. 1955. *Studies on the Cerebral Cortex (Limbic Structures)*, trans. L. M. Kraft. Chicago: Year Book
41. Valverde, F. 1965. *Studies of the Piriform Lobe.* Cambridge, Mass.: Harvard Univ. Press
42. Green, J. D., Mancia, M., von Baumgarten, R. 1962. *J. Neurophysiol.* 25:367
43. Yamamoto, C., Yamamoto, T., Iwama, K. 1963. 1. *Neurophysiol.* 26:403
44. Phillips, C. G., Powell, T. P. S., Shepherd, G. M. 1963. *J. Physiol.* 168:65
45. Shepherd, G. M. 1963. *J. Physiol.* 168: 101
46. Rall, W., Shepherd, G. M. 1968. *J. Neurophysiol.* 31:884
47. Freeman, W. J. 1969. *Physiologist* 12: 229
48. Freeman, W. J. 1970. In *Approaches to Neural Modeling*, ed. M. A. B. Brazier, D. Walter. Los Angeles: Brain Information Service, UCLA. In press
49. Eccles, J. C. 1957. *The Physiology of Nerve Cells*, Chaps. 2 (Fig. 21), 3 (Figs. 39, 45). Baltimore: JohnsHopkins
50. Granit, R., Kernell, D. Shortess, G. K. 1963. *J. Physiol.* 168:911
51. Rall, W. 1955. *J. Cell. Comp. Physiol.* 46:373
52. Ten Hoopen, M., Verveen, A. A. 1963. *Progr. Brain Res.* 2:8
53. Calvin, W. H., Stevens, C. F. 1968. *J. Neurophysiol.* 31:524

54. Freeman, W. J. 1967. *Physiologist* 10: 172
55. Parzen, E. 1960. *Modern Probability Theory and Its Applications*, p. 60. New York: Wiley
56. Freeman, W. J. 1971. Unpublished data
57. Freeman, W. J. 1968. *Math. Biosci.* 2: 181
58. Rall, W. 1960. *Exp. Neurol.* 2:503
59. Katz, B. 1939. *Electric Excitation of Nerve*. London: Oxford Univ. Press
60. Schwan, H. P. 1957. In *Advances in Biological and Medical Physics*, ed. J. H. Lawrence, C. A. Tobias, pp. 148-209. New York: Academic
61. Katz, B. 1966. *Nerve; Muscle, and Synapse*. New York: McGraw-Hill
62. Hodgkin, A. L., Rushton, W. A. H. 1946. *Proc. Roy. Soc. London* 133B:444
63. Rall, W. 1959. *Exp. Neurol.* 1:491
64. Eccles, J. C. 1964. *The Physiology of Synapses*. New York: Academic
65. Wall, P. D. 1962. *J. Physiol.* 164:508
66. Wilson, H. R., Cowan, J. D. 1972. *Biophys. J.* 12:1
67. Freeman, W. J. 1964. *Recent Advan. Biol. Psychiat.* 7:235
68. Emery, J., Freeman, W. J. 1969. *Physiol. Behav.* 4:69
69. Horowitz, J. M. 1972. *Electroencephalogr. Clin. Neurophysiol.* 32:227
70. Pickering, S., Freeman, W. J. 1968. *Exp. Neurol.* 19:127
71. Poggio, G. P., Vierristein, L. J. 1964. *J. Neurophysiol.* 27:517
72. Mimura, K., Sato, K. 1970. *Int. J. Neurosci.* 1: 75
73. Brazier, M. A. B. 1958. *The Electrical Activity of the Nervous System*. New York: MacMillan
74. John, E. R. 1967. *Mechanisms of Memory*. New York: Academic
75. Anderson, J. A. 1968. *Kybernetik* 5:113
76. Longuet-Higgins, H. C. 1968. *Proc. Roy. Soc. London.* 171B:327
77. Hubel, D. H., Wiesel, T. N. 1959. *J. Physiol.* 148:574
78. Mountcastle, V. B. 1961. In *Sensory Communication*, ed. W. A. Rosenblith, Cbap. 22. Cambridge: MIT Press
79. Barlow, H. B. 1969. In *Information Processing in the Nervous System*, ed. K. N. Liebovic, Cbap. 11. New York: Springer-Verlag

